Donor-acceptor control in grown-in-glass Ga-oxide nanocrystals by crystallization-driven heterovalent doping

Alberto Paleari,*[a,b] Nikita V. Golubev,[b] Elena S. Ignat'eva,[b] Vladimir N. Sigaev,[b] and Roberto Lorenzi[a]

Abstract: Incorporation of doping ions in nanocrystals is a strategy for providing nanophases with functions directly related to ion features. At the nanoscale, however, doping can also activate more complex effects mediated by perturbation of nanophase size and structure. Here we report a paradigmatic case in which we modify grown-in-glass γ-Ga_2O_3 nanophases via nickel or titanium doping of the starting glass, so as to control the concentration of oxygen and gallium vacancies responsible for the light emission. Optical absorption and luminescence show that Ni^{2+} and Ti^{4+} ions enter into the nanophase, but differential-scanning-calorimetry and x-ray-diffraction indicate that Ni and Ti also work as modifiers of nanocrystal growth. As a result, doping influences nanocrystal size and concentration, which in turn dictate the number of donors and acceptors per nanocrystal. Finally, the chain of effects turns out to control both intensity and spectral distribution of the light emission.

1. Introduction

Design and synthesis of nanostructures with specific functions require a deep understanding of growing mechanisms, kinetics, surface reactivity, and phase stability in the chemical environment of the process.[1] This is evident, for instance, in solution-based synthesis of quantum dots.[2] However, the potential complexity of the chemical and physical factors which determine the final nanostructure properties is even more compelling when we are dealing with nanocrystals (NCs) grown in a glass. In such systems, the players of the final material - nanophase, host, interphase, and possible dopant species - are included in the starting compound, *i.e.* the initial glass, and all these players find their final place thanks to multiple driving forces which cause and control NC nucleation and growth during post-synthesis treatments.[3]

In this field, some investigations have given relevant results in recent years, demonstrating the feasibility of glass-based easy-to-process nanostructured materials with different kinds of grown-in-glass NCs in transparent matrix - either from melting or by solution based methods. The investigated nanophases include oxides,[4-7] fluorides,[8-10] and metals.[11-13] Importantly, the resulting materials show to be suitable to be engineered for a wide range of applications, comprising optical 3D-memories,[13] UV-to-visible solar-blind converters,[14] special optical fibers,[15,16] and UV-emitting glassy-films.[7]

In glass-based nanostructured systems, a special role is played by wide-band-gap nano-oxides, since they can vehicle intrinsic and extrinsic functions into an optical silicate glass without compromising light transmittance in the visible range (provided that NC size is kept at few nm). Nanophases of Ga-oxides, in particular, are interesting as nanocrystalline hosts for broadband infrared-emitting transition metal ions,[17-23] and for their intense *e*-beam or UV excited blue emission.[14,24-34] Much of the interest is in the visible light emission which is efficiently excited at wavelengths shorter than 280 nm by band-to-band transitions, thanks to a direct allowed optical gap. The luminescence band is centred in the blue region at about 460 nm, but with more than one component. A spectral contribution comes from radiative recombination at donor and acceptor pairs (DAPs), with neutral oxygen vacancies V_O acting as donors, and complexes of oxygen and Ga vacancies $[V_O,V_{Ga}]^X$ behaving as acceptors.[35] Two additional components occur in the green and UV regions at 550 nm and just below 400 nm, ascribed to radiative transition at V_{Ga} sites and, respectively, from decay of self-trapped excitation probably mediated by sub-band gap levels as V_O sites.[35-39] Therefore, V_O and V_{Ga} sites turn out to govern spectral and kinetic features of light emission in Ga-oxide nanophases.

Starting from those results, some recent studies have demonstrated that DAP concentration per NC can be controlled, to some extent, by tailoring the NC size and, consequently, the concentration of V_O per NC at fixed oxygen deficiency in the nanophase. This result has been obtained either in nanopowder of selected size, or in grown-in-glass NCs by thermal tuning the nucleation process.[14,40,41] Nevertheless, V_O and V_{Ga} are expected to be also influenced by doping with ions substituting for Ga^{3+} with different oxidation state, as demonstrated in QD colloids,[42,43] so prospecting a size-independent method - driven by charge neutrality - to control the broadband visible light emission of Ga-oxide at the nanoscale. However, doping processes of nanophases, especially in grown-in-glass systems, may cause not negligible side effects on nanophase size and concentration. Such effects were in fact observed in Er-doped SnO_2 NCs in glass,[44] and have been analyzed in a recent study on lithium disilicates with transition metal doping.[45] Therefore, the development of a novel doping-induced strategy of DAP engineering in Ga-oxide nanophases needs data - for now still unavailable - about the possible effects of dopant species on the NC growth.

In the present work we report the analysis we have carried out on Ga-containing alkali-germanosilicate glasses perturbed by different levels of Ni^{2+} or Ti^{4+} doping, acting as oxygen stoichiometry modifiers (with opposite effects) inside Ga-oxide nanophases, as well as glass modifiers which promote atomic diffusion during nucleation, but also hinder NC growth forming blocking layers at the NC surfaces. The analysis of these factors,

[a] Prof. A. Paleari, Dr. R. Lorenzi
Department of Materials Science.
University of Milano-Bicocca
via R. Cozzi 55, 20125 Milano (Italy)
E-mail: alberto.paleari@unimib.it
[b] Prof. V.N. Sigaev, Dr. N.V. Golubev, Dr. E.S. Ignat'eva
P.D. Sarkisov Int. Laboratory of Glass-based Functional Materials
Mendeleev University of Chemical Technology of Russia
Miusskaya Square 9, 125190 Moscow (Russia)

Supporting information for this article is given via a link at the end of the document.

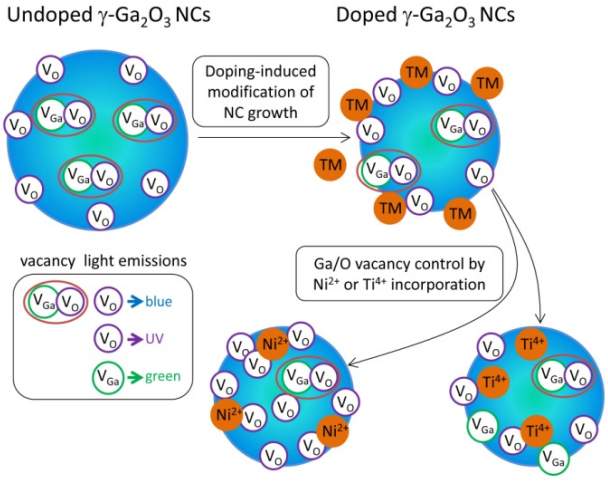

Figure 1. Strategy of doping-driven control of NC size and population of Ga and O vacancies in grown-in-glass γ-Ga_2O_3, mediated by glass viscosity lowering, diffusion blocking barriers, and Ni^{2+} and Ti^{4+} incorporation. Box on the left: light emitting centers.

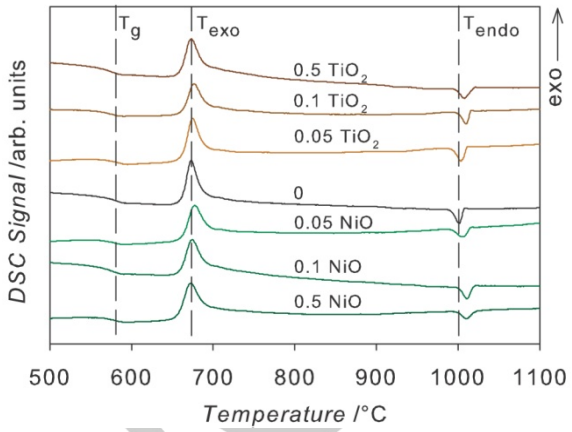

Figure 2. DSC curves of 7.5Li_2O-2.5Na_2O-20Ga_2O_3-45GeO_2-25SiO_2 (mol%) glasses undoped and doped with the indicated molar amount of NiO or TiO_2. Curves are shifted for clarity. Temperature of glass transition (T_g), γ-Ga_2O_3 nano-crystallization (T_{exo}), and decomposition of $LiGa_5O_8$ NCs with formation of β-Ga_2O_3 (T_{endo}) are indicated by dashed lines for undoped material.

which affect the formation of γ-Ga_2O_3 NCs in the glass matrix and the population of Ga and O vacancies inside NCs (Figure 1 and Section S1 in Supporting Information), gives at last a basis for tailoring the concurring effects of DAP engineering and NC size control.

2. Results and Discussion

2.1. Doping Effects on Nanocrystallization

The analysis of differential-scanning-calorimetry (DSC) and x-ray diffraction (XRD) data gives us evidence of detectable structural effects caused by Ni and Ti doping. In Figure 2, we report DSC curves of glass samples with composition 7.5Li_2O-2.5Na_2O-20Ga_2O_3-45GeO_2-25SiO_2, either undoped or doped with different NiO or TiO_2 molar content. In all the compositions we register the occurrence of three main features - a smooth step at the glass transition temperature in the range 560-590 °C, an exothermic peak with maximum in the temperature range 673-677 °C, and an endothermic process at about 1000-1010 °C.

In agreement with other studies on similar compositions,[3,46] the exothermic peak is related to the process of nano-crystallization of γ-Ga_2O_3 in the glass matrix, while the endothermic peak is caused by NC decomposition after transformation into $LiGa_5O_8$ by Li-diffusion, with final formation of β-Ga_2O_3 NCs. Besides these shared features, the DSC curves of both Ni and Ti-doped samples show some differences from the curve of the undoped composition, consisting in small but clear shifts of the glass transition temperature T_g (Figure 3a) and of the exothermic and endothermic peaks at T_{exo} and T_{endo} (Figures 3b and 2c). The detected shifts indicate that doping does really influence some of the processes occurring in the glass during the thermal treatment.

Different factors can affect the glass transition and the crystallization steps inside a complex glass. In fact, transition metal ions tend to gather at the NC growing front, so forming a barrier to atomic diffusion during phase separation and NC growth as recently demonstrated in doped lithium disilicate systems.[45]

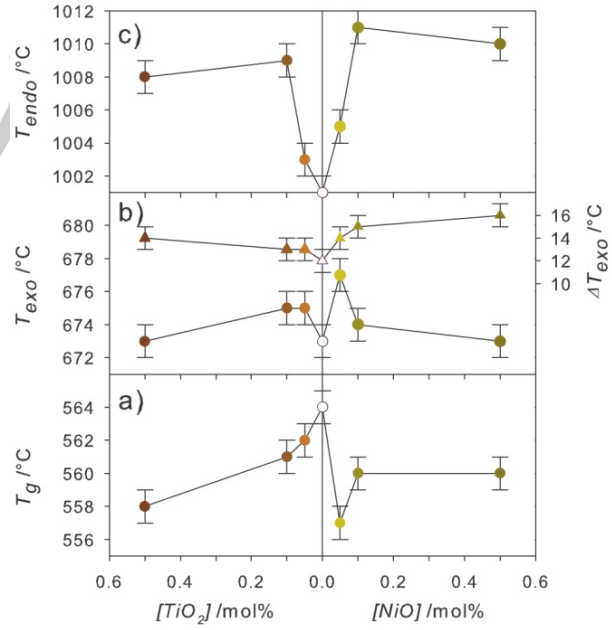

Figure 3. a) Glass transition temperature (T_g) in samples with different content of added TiO_2 or NiO compared with undoped composition (empty circle); b) maximum peak temperature of the exothermic process of γ-Ga_2O_3 nano-crystallization (T_{exo}, left axis) and difference ΔT_{exo} (triangles, right axis) between the onset temperature of the exothermic process and T_{exo}; c) peak temperature of the endothermic process of decomposition of Li-diffused NCs with formation of β-Ga_2O_3.

In fact, in nanophases, it is thermodynamically unfavourable for the dopant to enter in the NC. Therefore, dopant species are preferably excluded from the NC 'bulk' and located onto the nanoparticle surface.[47] Such an effect can decrease the rate of diffusion during NC growth and leads to the broadening and shift of the exothermic peak as we register in Figure 3b. Weaker effects of TiO_2 with respect to NiO doping are consistent with a more pronounced tendency of Ti atoms to act as a glass former, and with a larger amount of Ti in the glass which does not contribute to the formation of diffusion blocking layers around growing NCs. Furthermore, the larger radius of Ni^{2+} ions (0.069 nm) with respect to Ga^{3+} and Ti^{4+} (0.062 and 0.0605 nm,[48] respectively) leads to higher propensity to accumulate at the interface and to form diffusion blocking layer around growing NCs. Such a view is also compatible with the larger availability of octahedral sites at NC surface than in bulk,[49] so giving to Ni^{2+} ions a preferential accommodation at NC surface (much more than to Ti^{4+} ions which easily admit tetrahedral sites). At high doping levels, the more pronounced doping-induced change of composition affects glass viscosity (as indicated by lower T_g in Figure 3a) and favours diffusion, so as to shift the crystallization process to lower temperature.

The temperature shift of the irreversible endothermic process of NC decomposition (Figure 3c) is an additional evidence of the modified matrix viscosity by Ni and Ti doping.

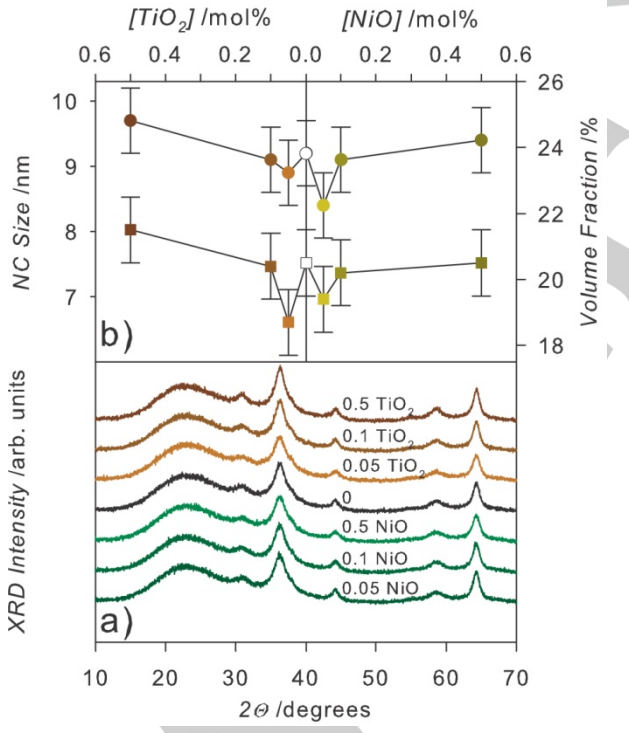

Figure 4. a) XRD patterns of $7.5Li_2O$-$2.5Na_2O$-$20Ga_2O_3$-$45GeO_2$-$25SiO_2$ glasses (mol%) undoped and doped with NiO or TiO_2 after heating 10 °C min^{-1} from 20 to 675 °C and 15 min at the final temperature. Curves are shifted for clarity. b) NC size (circles, left axis) and volume fraction of crystallized material (squares, right axis) *vs.* doping level from XRD analysis.

We know, in fact, that the temperature of the endothermic process at about 1000 °C mainly depends on the final $LiGa_5O_8$ NC size which results from mechanisms of NC coalescence and Li embedding occurring at temperature above T_{exo}.[46] Specifically, the larger the NC size, the higher the temperature of the endothermic peak. Since NC coalescence and Li diffusion are promoted by viscosity lowering, the higher the doping - with lower glass viscosity - the larger the size of $LiGa_5O_8$ NCs. The data in Figure 3c substantially confirms this view, showing increasing T_{endo} at increasing doping levels, at least up to 0.1 mol%. Heavy doping probably induce a large defectiveness which destabilizes NCs so as to compensate the stabilizing effects caused by larger NC sizes (see also Figures S1 and S2 in Section S2 of supporting information).

In Fig. 4(a), we report XRD patterns after treatment at the exothermic peak of γ-Ga_2O_3 crystallization. We observe reflections ascribable to γ-Ga_2O_3, with relative intensities intermediate between two PDF files (PDF 01-074-7709 and PDF 00-020-0426). Different PDF files are in fact reported in databases for γ-Ga_2O_3 - synthesized only as nanopowders or colloidal systems - reflecting a strong propensity to structural disorder in the occupation of octahedral and tetrahedral spinel sites by Ga^{3+} ions,[49] and to the incorporation of Li^+ ions substituting for Ga^{3+} ions.

Besides the identification of the crystallized phase, the analysis of the XRD patterns seems to show some differences in crystalline volume fraction and NC size by changing the doping level. Actually, most of the registered changes are comparable with the experimental uncertainty. However, especially in the data of Ti-doped samples, there is some evidence of slightly smaller NC size and crystalline fraction at low doping level with respect to undoped material, followed by larger values at higher doping, with a behaviour similar to the behaviour of T_{exo} shift in Figure 3b. This result suggests the occurrence of a doping-related hindering of NC growth at the lowest doping level. Diffusion blocking effect of dopant species at the surface of growing crystals can prevail over doping-induced glass viscosity lowering which should favour NC growth with respect to the undoped composition. Instead, at heavier doping, the expected effects caused by the decrease of viscosity probably prevails, as suggested by slightly larger values of NC size and volume fraction.

In summary, the analysis of DSC and XRD data shows that Ni and Ti doping can influence the glass nanocrystallization, with effects on size and concentration of γ-Ga_2O_3 NCs. Therefore, since NC size affects the balance between V_O and V_{Ga} sites inside each NC,[41] we can expect a NC size-related effect of doping on the donor-acceptor light emission properties of NCs. Furthermore, Ti^{4+} and Ni^{2+} ions substituting for Ga^{3+} can also play an even larger and more direct role in DAP and defect-related optical emissions of the nanophase, provided that they enter into NCs so as to modify donor and acceptor population by heterovalent substitution. In the next sections we analyze optical absorption and light emission data giving us evidence of incorporation of the ions in NCs and modification of the donor and acceptor ratio.

2.2. Incorporation of Ni in Nanocrystals

In Figure 5a, we report the optical absorption spectra of NiO-doped nanostructured glassceramics in the visible and near UV region. At energy lower than 4 eV, below the absorption edge caused by band-to-band transitions of γ-Ga_2O_3 NCs and by high-energy charge-transfer (CT) transitions at Ni-O bonds,[50] we register two main absorption bands at 1.96 and 3.25 eV.

These bands are ascribable to the crystal-field transitions $^3A_2(F)\rightarrow{}^3T_1(F)$ and $^3A_2(F)\rightarrow{}^3T_1(P)$ of Ni^{2+} ions in octahedral environment,[51] substituting for Ga^{3+} in octahedral spinel sites of γ-Ga_2O_3 NCs. These bands are not observed in as quenched glass, where Ni^{2+} ions are dispersed in the amorphous matrix in lower symmetry sites giving rise to an intense band at 2.86 eV. Importantly, the 2.86 eV band is not detected in nanostructured materials or, if any, is hidden in the low energy tail of the 3.25 eV band, which instead increases proportionally to the NiO content, according to the Lambert-Beer law, as the 1.96 eV band (inset in Fig. 5(a)). The quantitative analysis of this outcome allows us to give a lower limit of more than 90% of the total Ni^{2+} ions incorporated into the nanophase, without saturation effects.

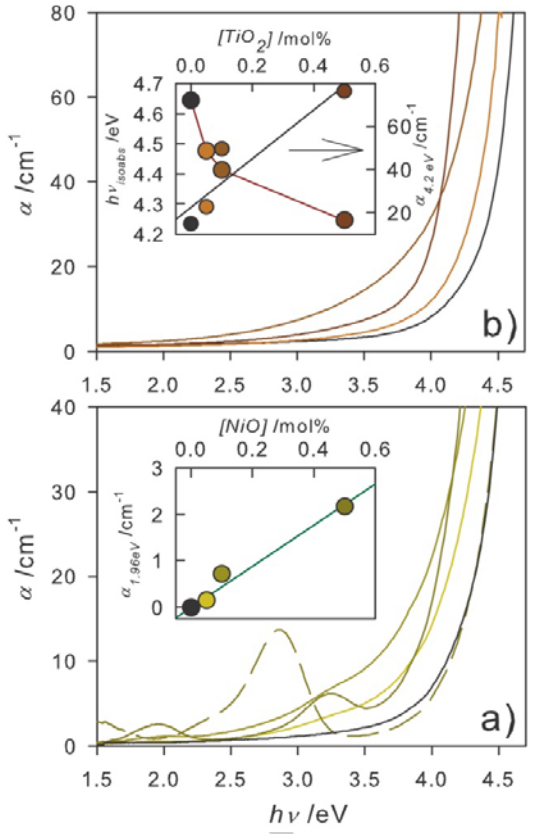

Figure 5. a) Optical absorption spectra of NiO-doped nanostructured glass-ceramics compared with undoped material and 0.5 mol% NiO doped as quenched glass (dashed line). Inset: absorption coefficient at the maximum of the band at 1.96 eV as a function of the NiO content. (b) Optical absorption spectra of TiO_2-doped nanostructured glassceramics compared with undoped material. Inset: (left axis) doping dependence of the photon energy at which the absorption coefficient is equal to an arbitrary reference value of 80 cm^{-1}; (right axis) doping dependence of the absorption coefficient at 4.2 eV. Experimental uncertainty is within the symbol size.

2.3. Incorporation of Ti in Nanocrystals

The absorption spectra of TiO_2-doped glassceramics do not show detectable traces of crystal field or defect-related transitions below the absorption edge of γ-Ga_2O_3 NCs. This fact tells us about the titanium oxidation state, which is Ti^{4+} independently of doping level or nanostructuring treatment, since Ti^{3+} would give rise to transitions in the visible region at about 500 nm.[52] The doping-related shift of the UV absorption edge can instead provide some information on the environment of Ti^{4+} sites. Different factors can be responsible for the shift, such as NC size effects on the energy gap (potentially driven by TiO_2 in the matrix, Figure 4b), the increase of crystalline fraction (dependent on TiO_2 addition, Figure 4b) and the consequent increase of intensity of the UV absorption tail, the energy gap lowering by enhancement of oxygen mean polarizability (dependent on TiO_2 incorporation in NCs), and the superposition of $O^{2-}\rightarrow Ti^{4+}$ CT transitions (at energy dependent on Ti^{4+} coordination).

Actually, we can rule out NC size effects on the energy gap. In fact, the expected change $\delta(\Delta E_G)$ of the size-dependent shift ΔE_G of the energy gap E_G is less than 10^{-2} eV in the size range 9-10 nm (from 2R data in Figure 4b), as determined by the expression $\Delta E_G=(\hbar^2\pi^2/2m^*R^2)-1.8e^2/4\pi\varepsilon R$,[53] where m* is the reduced exciton mass (about 0.3 electron mass in Ga_2O_3),[54] ε is dielectric function (about $10\varepsilon_0$),[55] and R is the NC radius. Similarly, the slight increase of crystalline fraction with increasing TiO_2 content (less than 5%, data in Figure 4b) cannot explain the enhancement by a factor 4 of the absorption coefficient at fixed energy (inset in Figure 5b, right axis). As regards the possible narrowing of Ga_2O_3 E_G by incorporation of Ti oxide in NCs, we can estimate the order of magnitude of the expected effect from the empirical Duffy's relation $E_G=20(1-R_m/V_m)^2$ between E_G and the ratio between the molar refraction R_m and the molar volume V_m.[56,57] In fact, R_m is directly related to the molar polarizability α_m of the material, which can in turn be calculated additively from the reported molar polarizability of the simple oxides Ga_2O_3 and TiO_2.[57] In this way, we estimate a shift of E_G of only -4×10^{-2} eV from undoped to 0.5 mol% TiO_2 doped Ga_2O_3, to be compared with a shift of about 0.4 eV in the iso-absorption energy observed at 80 cm^{-1} of absorption coefficient (Figure 5b, left axis). Therefore, the most reliable interpretation of the observed change of UV absorption edge must be based on $O^{2-}\rightarrow Ti^{4+}$ CT transitions contributing to the near UV absorption edge together with the onset of Ga-oxide band-to-band excitations. Such attribution is consistent with the observed linear dependence of the absorption coefficient at fixed energy on the TiO_2 content (inset in Figure 5b, right axis). Furthermore, the spectral position of the steep doping-dependent absorption tail suggests that the Ti-related band probably lies in the range 4.5-5 eV. This spectral range is consistent with $O^{2-}\rightarrow Ti^{4+}$ CT bands observed in other systems with Ti^{4+} ions in six-fold or five-fold coordination, as in crystals or glassceramics.[58] By contrast, in glass, $O^{2-}\rightarrow Ti^{4+}$ CT bands from four-fold sites are expected, with spectral position lying at higher energy, in agreement with the bathochromic effect (i.e. a red-shift) already registered in Ti^{4+} CT transitions at increasing Ti^{4+} coordination number in

zeolites.[59] Therefore, the data in Figure 5 suggests that a fraction of Ti^{4+} ions are incorporated in γ-Ga_2O_3 NCs in octahedral sites substituting for Ga^{3+} ions. In the next section we show that Ti^{4+} and Ni^{2+} incorporation in NCs has also outcomes in the NC light emission.

2.4. Doping Effects on Light Emission

The evidences of NC size effects after NiO and TiO_2 addition (Figure 4) and the indication of Ni^{2+} and Ti^{4+} incorporation in NCs (Figure 5) are accompanied by doping-related effects on the NC light emission properties. Indeed, we observe effects both on the spectral distribution of the light emission and on the integrated intensity. To analyze the doping related spectral changes, we report in Figures 6a and 6b the normalized photoluminescence (PL) spectra of NiO- and TiO_2-doped nanostructured glassceramics, respectively, compared with the undoped composition. The resulting colour actually shows more evident changes in TiO_2-doped materials, with a shift from blue to almost white emission. We analyze the changes as effects of dopant ions on distinct light emitting centres.

We report in Figure 7 the analysis of the spectral distribution of emitted power as a superposition of three Gaussian components, with intensities as free parameters. In the analysis, spectral positions and bandwidths are empirically constrained using the spectra of undoped and heavy doped materials.

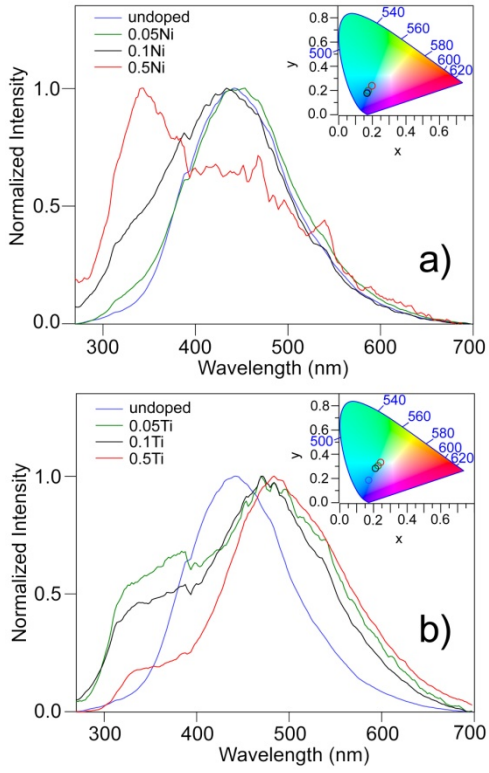

Figure 6. PL spectra excited at 250 nm, at room temperature, in glassceramic 7.5Li_2O-2.5Na_2O-20Ga_2O_3-45GeO_2-25SiO_2 (mol%) undoped and doped with the indicated molar amount of a) NiO and b) TiO_2. Insets: chromaticity coordinates of the spectra in the CIE-1931 colour space (marks are in the same colour of spectra).

In fact, the low energy side of the main blue peak in the undoped sample and, respectively, the low energy and the central portion of green and UV bands in doped materials can be satisfactorily fitted by Gaussian components either directly (for the blue band) or after subtraction of the previously fitted blue component (for green and UV bands). We obtain Gaussian components centred at 2.47, 2.89, and 3.75 eV - with bandwidth σ 0.24, 0.33, and 0.33 eV, respectively. The analysis in three components is consistent with the occurrence of previously identified mechanisms of UV, blue, and green emission in Ga oxide systems, respectively ascribed to decay of self-trapped excitation, DAP recombination, and radiative transition at V_{Ga} sites.[27,35-39] Even the spectral parameters are consistent with previous analyses, provided that one takes into account the change of spectral distributions from PL intensity spectra to emitted power spectra we calculated as PL signal intensity divided by the squared wavelength.[60] The results of this analysis in TiO_2-doped material (Figures 7b-d) register a strong doping-induced lowering of intensity of the blue component with respect to the undoped glassceramic (Figure 7a).

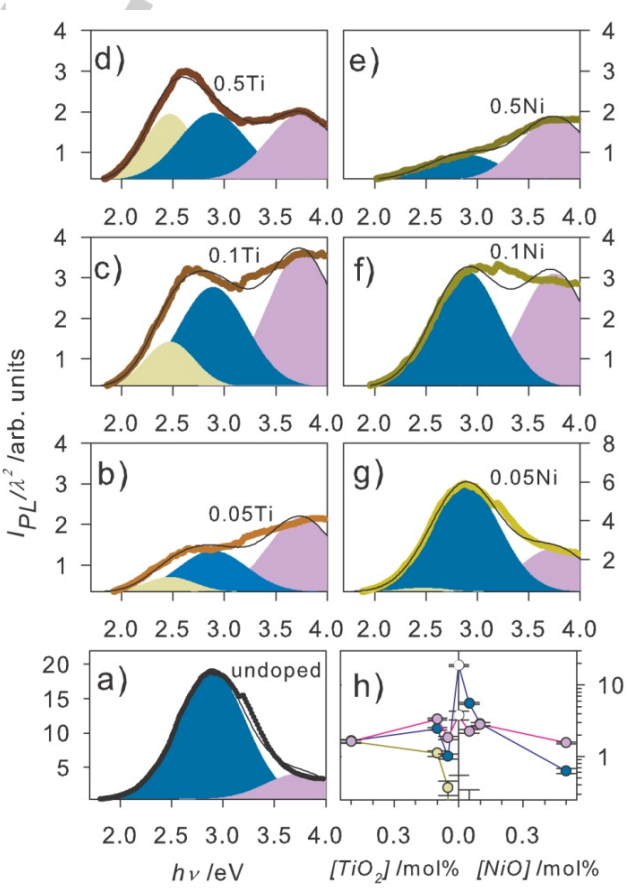

Figure 7. Spectra of emitted light power vs. photon energy (circles) and fit (lines) as sum of three Gaussian components (filled areas) with fixed spectral parameters (see text) in nanostructured 7.5Li_2O-2.5Na_2O-20Ga_2O_3-45GeO_2-25SiO_2 (mol%) glassceramics a) undoped, and doped with b) 0.05 mol% TiO_2, c) 0.1 mol% TiO_2, d) 0.5 mol% TiO_2, e) 0.5 mol% NiO, f) 0.1 mol% $ NiO, g) 0.05 mol% NiO. h) Amplitudes of the three Gaussian components as a function of the doping level (same colour codes as in a)-g)).

This is consistent with a strong effect of TiO_2 in hindering the formation of $[V_O,V_{Ga}]^X$, which are the acceptor sites responsible for the blue emission in DAP recombination. Such an effect can result from Ti^{4+} incorporation in NCs with partial compensation for the charge unbalance by V_{Ga} sites, so as to prevent V_O and V_{Ga} sites from forming complexes (see also Section S1 in Supporting Information). According to this mechanism, the process of Ti^{4+} incorporation makes a fraction of V_{Ga} sites free to act as independent light emitting localized defects, whose emission is responsible for the green PL component. In fact, parallel to the bleaching of the blue component, we register the appearance and increase of the green emission with TiO_2 addition (Figures 7a-d). By contrast, the UV band - related to the occurrence of V_O sites - does not change so much as the other two components. This fact indicates that the relative decrease of V_O sites with increasing TiO_2 addition is not particularly relevant, even though it significantly affects the number of $[V_O,V_{Ga}]^X$ complexes, consistently with the natural tendency of Ga oxides to oxygen deficiency rather than cation non-stoichiometry. Interestingly, in 0.5 mol% TiO_2 doped material (Figure 7d), the intensities of the three components are almost equal and give rise to a quite broad light emission. All these data are summarized in Figure 7h as a function of TiO_2 content.

The effects of NiO doping are quite different with respect to TiO_2. The intensity of the blue emission decreases with doping more gradually (Figures 7a, 7e-g), but with a more relevant final decrease at large NiO content. This behaviour is consistent with an effect of Ni^{2+} incorporation in NCs on the yield of DAP recombination. In fact, increasing the number of Ni substituted sites we expect - for charge neutrality - an increase of V_O, which in turn enhance the probability of radiative and nonradiative decay paths competitive to DAP recombination.[14,40] This view fits also the lack of relevant contribution in the green component of the spectrum, ruling out a significant influence of doping on the population of V_{Ga} sites and their pairing to V_O sites. Instead, UV emission shows minor changes, as in TiO_2-doped material.

It is worth noting that the effects of TiO_2 or NiO doping on NC size and crystalline fraction are far from playing a role on the light emission properties at least comparable with those of Ti^{4+} and Ni^{2+} ions as modifiers of the ratio between V_{Ga} and V_O sites inside the NCs. In fact, the reduction of NC size, which is expected to increase DAP recombination yield,[14,40] is evidently overwhelmed by the other mechanisms, since opposite effects are observed in samples where we register smaller NC size than in undoped material (data at low doping in Figure 4b and Figure 7h). Similarly, the expected effects on the PL spectrum from the relatively small increase of crystalline fraction - from the lowest doping level to higher values (Figure 4b) - can hardly justify the observed change of light emission intensity in Figures 7b-g, and even more the complex change of relative intensity of the different components. Interestingly, the role of V_O and V_{Ga} relative population on the observed spectral changes caused by TiO_2 or NiO doping is instead supported by PL measurements of undoped variants of glassceramics samples we obtained from glass melted in different oxygen atmosphere (Figure S3 in Supporting Information), in which we register spectral changes similar to those in Figure 6.

Conclusions

The analysis of structural and optical features of grown-in-glass γ-Ga_2O_3 NCs allows us to draw now a quite articulated picture of the potential of TiO_2 and NiO doping for tailoring the nano-crystallization process of Ga-oxides in alkali-germanosilicate glass matrix so as to modify size and relative amount of the nanophase and to drive concentration and balance of the main light emitting intrinsic sites. Importantly, while we register clear effects of TiO_2 and NiO as glass modifiers able to determine the final NC size and fraction of crystalline nanophase, we can also confirm that the doping species are incorporated in NCs to some extent (completely in the case of NiO) and actively work as modifiers of the NC stoichiometry acting as Ni^{2+} and Ti^{4+} substituting ions for Ga^{3+} in octahedral sites. Furthermore, the analysis of the spectral distribution of light emission as a function of doping demonstrates that Ti^{4+} and Ni^{2+} ions effectively change the balance between V_{Ga} and V_O and, consequently, the relative weight of the main optically active sites responsible for PL in the nanostructured material. The data indicates that the direct effects of incorporated species on the light emission (through the change of V_{Ga} and V_O populations) are much more relevant than the indirect effects (via NC size change) previously observed in undoped material and related on the influence of NC size and growth on DAP population and kinetics. Our new results show that DAP recombination and localized transitions at oxygen and gallium vacancy sites can be largely tailored by Ni^{2+} and Ti^{4+} substituting for Ga^{3+}, with relevant changes of the resulting spectral distribution of light emission, as a result of the control of three concomitant spectral contribution in the UV, blue and green regions, ascribable to some extent to the relative population of V_O, DAP and V_{Ga} sites, respectively.

Experimental Section

Sample Preparation

We prepared glass samples by melt-quenching method, with nominal composition $7.5Li_2O$-$2.5Na_2O$-$20Ga_2O_3$-$45GeO_2$-$25SiO_2$ (mol%). We used, as raw materials, amorphous SiO_2 (special purity grade), GeO_2 (special purity grade), Li_2CO_3 (chemically pure), Na_2CO_3 (chemically pure), Ga_2O_3 (chemically pure). Glasses with composition different from the abovementioned one were also synthesized by introducing different amount (0.05, 0.10, 0.50 mol%) of NiO or TiO_2 reagents (chemically pure). The amount of reagents in each batch was calculated in order to prepare 70 g of final product. The starting materials were weighed using an analytical balance with an accuracy of 1 mg. In each preparation, the raw powders were thoroughly hand mixed in a beaker for 15-20 min. The glasses were prepared in an uncovered platinum crucible (about 45 ml) in an electrically heated furnace at a temperature of 1480 °C for 40 min. The melt was poured onto a stainless steel plate and quenched by pressing with another stainless steel plate to obtain samples of about 2 mm of thickness. The as-quenched glass was cut to the desired shape with a low-speed diamond saw or grinding disc using water as a coolant. Samples were then polished for optical measurements or ground for powder diffraction. Part of the as-quenched bulk samples was heat-treated in a muffle at 675 °C according to data obtained from DSC

analysis. In such cases, heat treatments were performed, with an accuracy of the temperature control within ±2 °C, placing the samples into the furnace at room temperature and heating at a rate of 10 °C min^{-1}. After treatment, the samples were quenched removing them from the furnace after stay for 15 min at the DSC peak extremum temperature.

Physical Measurements

DSC measurements from room temperature up to 1200 °C were performed on a Netzsch DSC 449F3 high-temperature thermoanalyzer in platinum pan with cover, at a heating rate of 10 °C min^{-1} in Ar, using bulk samples of 15-20 mg. The reproducibility of endothermic and exothermic peak extremum temperature is within 2 °C. X-ray diffraction patterns of powdered samples were recorded on a D2 Phaser diffractometer (Bruker) employing nickel-filtered CuK_α radiation. Crystalline phases were identified by comparing peak position and relative intensities in the XRD pattern with the ICDD PDF-2 database. Mean NC size was estimated from Scherrer's analysis of the width of XRD reflections, after numerical subtraction of the background and amorphous halo from the whole XRD pattern and fitting nanophase reflections, using the software Diffrac.Eva by Bruker. Crystallized fraction was estimated as $100(1-(A_x-A_p)/A_x)$, where A_x and A_p are respectively the area of the whole XRD pattern (without background) and the area of the peaks. Optical absorption spectra were collected by means of a Cary 50 (Varian) spectrophotometer with 1 nm resolution from 200 to 1000 nm. Photoluminescence (PL) spectra were taken exciting at 250 nm using a xenon lamp and a MS2004i (SOL instruments Ltd) monochromator with a bandwidth of 4 nm and collecting the emitted light through a second monochromator MS3504i (SOL instruments Ltd) with a spectral resolution of 2 nm and a photosensor module H7844 (Hamamatsu).

Acknowledgements

This work has been supported by the Ministry of Education and Science of the Russian Federation under Grant 14.Z50.31.0009 and by Grant MK-8807.2016.3, by Cariplo Foundation, Italy, under Project 2012-0920 and Grant 2014-1971.

Keywords: donor-acceptor systems • doping • glasses • nanocrystals • photophysics

[1] J. A. Hollingsworth, V. I. Klimov, in *Semiconductor and metal nanocrystals* (Ed. V. I. Klimov), Marcel Dekker, New York, **2004**, pp. 1-64.
[2] C. B. Murray, C. R. Kagan, M. G. Bawendi, *Annu. Rev. Mater. Sci.* **2000**, *30*, 545-610.
[3] V. N. Sigaev, N. V. Golubev, E. S. Ignat'eva, B. Champagnon, D. Vouagner, E. Nardou, R. Lorenzi, A. Paleari, *Nanoscale* **2013**, *5*, 299-306.
[4] S. Zhou, C. Li, G. Yang, G. Bi, B. Xu, Z. Hong, K. Miura, K. Hirao, J. Qiu, *Adv. Funct. Mater*. **2013**, *23*, 5436-5443.
[5] S. Zhou, N. Jiang, B. Wu, J. Hao, J. Qiu, *Adv. Funct. Mater.* **2009**, *19*, 2081-2088.
[6] S. Chenu, E. Véron, C. Genevois, G. Matzen, T. Cardinal, A. Etienne, D. Massiot, M. Allix, *Adv. Optical Mater.* **2014**, *2*, 364-372.
[7] S. Brovelli, N. Chiodini, R. Lorenzi, A. Lauria, M. Romagnoli, A. Paleari, *Nature Commun.* **2012**, *3*, 690/1-9.
[8] A. C. Yanes, A. Santana-Alonso, J. Méndez-Ramos, J. del-Castillo, V. D. Rodríguez, *Adv. Funct. Mater.* **2011**, *21*, 3136-3142.
[9] G. Dantelle, M. Mortier, D. Vivien, G. Patriarche, *Chem. Mater.* **2005**, *17*, 2216-2222.
[10] S. Zhou, N. Jiang, K. Miura, S. Tanabe, M. Shimizu, M. Sakakura, Y. Shimotsuma, M. Nishi, J. Qiu, K. Hirao, *J. Am. Chem. Soc.* **2010**, *132*, 17945-17952.
[11] V. N. Sigaev, V. I. Savinkov, S. V. Lotarev, G. Yu. Shakhgildyan, R. Lorenzi, A. Paleari, *Nanotech.* **2013**, *24*, 225302/1-10.
[12] G. Lin, H. Pan, J. Qiu, Q. Zhao, *Chem. Phys. Lett.* **2011**, *516*, 186-191.
[13] A. Royon, K. Bourhis, M. Bellec, G. Papon, B. Bousquet, Y. Deshayes, T. Cardinal, L. Canioni, *Adv. Mater.* **2010**, *22*, 5282-5286.
[14] V. N. Sigaev, N. V. Golubev, E. S. Ignat'eva, A. Paleari, R. Lorenzi, *Nanoscale* **2014**, *6*, 1763-1774.
[15] V. M. Mashinsky, N. M. Karatun, V. A. Bogatyrev, V. N. Sigaev, N. V. Golubev, E. S. Ignat'eva, R. Lorenzi, M. C. Mozzati, A. Paleari, E. M. Dianov, *Microsc. Microan.* **2012**, *18*, 259-265.
[16] A. S. Zlenko, V. M. Mashinsky, L. D. Iskhakova, S. L. Semjonov, V. V. Koltashev, N. M. Karatun, E. M. Dianov, *Optics Express* **2012**, *20*, 23186-23200.
[17] S. Zhou, H. Dong, G. Feng, B. Wu, H. Zeng, J. Qiu, *Opt. Express* **2007**, *15*, 5477-5481.
[18] S. Zhou, G. Feng, B. Wu, N. Jiang, S. Xu, J. Qiu, *J. Phys. Chem. C* **2007**, *111*, 7335-7338.
[19] B. Wu, S. Zhou, J. Ren, D. Chen, X. Jiang, C. Zhu, J. Qiu, *Appl. Phys. B* **2007**, *87*, 697-699.
[20] S. Xu, D. Deng, R. Bao, H. Ju, S. Zhao, H. Wang, B. Wang, *J. Opt. Soc. Am. B* **2008**, *25*, 1548-1552.
[21] V. N. Sigaev, N. V. Golubev, E. S. Ignat'eva, V. I. Savinkov, M. Campione, R. Lorenzi, F. Meinardi and A. Paleari, *Nanotechnology* **2012**, *23*, 015708/1-7.
[22] S. V. Lotarev, A. S. Lipatiev, N. V. Golubev, E. S. Ignat'eva, G. E. Malashkevich, A. V. Mudryi, Yu. S. Priseko, R. Lorenzi, A. Paleari, V. N. Sigaev, *Optics Lett.* **2013**, *38*, 492-494.
[23] X. Duan, D. Yuan, X. Cheng, Z. Liu, X. Zhang, *J. Alloys Compd.* **2008**, *453*, 379-381.
[24] S. C. Vanithakumari, K. K. Nanda, *Adv. Mater.* **2009**, *21*, 3581-3584.
[25] T. Chen, K. Tang, *Appl. Phys. Lett.* **2007**, *90*, 053104/1-3.
[26] L. C. Tien, C. H. Ho, X. T. Yao, J. R. Cai, *Appl. Phys. A* **2011**, *102*, 105-108.
[27] K. Shimamura, E. G. Víllora, T. Ujiie, K. Aoki, *Appl. Phys. Lett.* **2008**, *92*, 201914/1-3.
[28] Z. Liu, X. Jing, L. Wang, *J. Electrochem. Soc.* **2007**, *154*, H440-H443.
[29] C. -C. Huang, C. -S. Yeh, *New J. Chem.* **2010**, *34*, 103-107.
[30] T. Wang, P. V. Radovanovic, *Chem. Commun.* **2011**, *47*, 7161-7163.
[31] T. Wang, S. S. Farvid, M. Abulikemu, P. V. Radovanovic, *J. Am. Chem. Soc.* **2010**, *132*, 9250-9252.
[32] S. S. Farvid, T. Wang, P. V. Radovanovic, *J. Am. Chem. Soc.* **2011**, *133*, 6711-6719.
[33] S. I. Maximenko, L. Mazeina, Y. N. Picard, J. A. Freitas Jr, V. M. Bermudez, S. M. Prokes, *Nano Lett.* **2009**, *9*, 3245-3251.
[34] R. Lorenzi, A. Paleari, N. V. Golubev, E. S. Ignat'eva, V. N. Sigaev, M. Niederberger, A. Lauria, *J. Mater. Chem. C* **2015**, *3*, 41-45.
[35] L. Binet, D. Gourier, *J. Phys. Chem. Solids* **1998**, *59*, 1241-1249.
[36] J. Díaz, I. López, E. Nogales, B. Méndez, J. Piqueras, *J. Nanopart. Res.* **2011**, *13*, 1833-1839.
[37] T. Harwig, F. Kellendonk, S. Slappendel, *J. Phys. Chem. Solids* **1978**, *39*, 675-680.
[38] G. Blasse, A. Bril, *J. Phys. Chem. Solids* **1970**, *31*, 707-711.
[39] V. V. Vasil'tsiv, Ya. M. Zakharko, *Sov. Phys. Solid State* **1983**, *25*, 72-74.
[40] M. Hegde, T. Wang, Z. L. Miskovic, P. V. Radovanovic, *Appl. Phys. Lett.* **2012**,*100*, 141903/1-5.
[41] N. V. Golubev, E. S. Ignat'eva, V. N. Sigaev, L. De Trizio, A. Azarbod, A. Paleari, R. Lorenzi, *J. Mater. Chem. C* **2015**, *3*, 4380-4387.
[42] J. Z. Zhang, J. K. Cooper, S. Gul, *J. Phys. Chem. Lett.* **2014**, *5*, 3694-3700.
[43] M. Kuno, *J. Phys. Chem. Lett.* **2014**, *5*, 3817-3818.

[44] S. Brovelli, A. Baraldi, R. Capelletti, N. Chiodini, A. Lauria, M. Mazzera, A. Monguzzi, A. Paleari, *Nanotech.* **2006**, *17*, 4031-4036.
[45] K. Thieme, I. Avramov, C. Rüssel, *Sci. Rep.* **2016**, *6*, 25451/1-16.
[46] N. V. Golubev, E. S. Ignat'eva, V. N. Sigaev, A. Lauria, L. De Trizio, A. Azarbod, A. Paleari, R. Lorenzi, *Phys. Chem. Chem. Phys.* **2015**, *17*, 5141-5150.
[47] H. Hodes, *Adv. Mater.* **2007**, *19*, 639-655.
[48] R. D. Shannon, *Acta Cryst.* **1976**, *A32*, 751-767.
[49] H. Y. Playford, A. C. Hannon, M. G. Tucker, D. M. Dawson, S. E. Ashbrook, R. J. Kastiban, J. Sloan, R. I. Walton, *J. Phys. Chem. C* **2014**, *118*, 16188-16198.
[50] T. Sakurai, M. Ishigame, H. Arashi, *J. Chem. Phys.* **1969**, *50*, 3241-3245.
[51] O. S. Dymshits, A. A. Zhilin, T. I. Chuvaeva, M. P. Shepilov, *J. Non-Cryst. Sol.* **1991**, *127*, 44-52.
[52] N. A. El-Shafi, M. M. Morsi, *J. Mater. Sci.* **1997**, *32*, 5185-5189.
[53] L. Brus, *J. Phys. Chem.* **1986**, *90*, 2555-2560.
[54] H. He, R. Orlando, M. A. Blanco, R. Pandey, E. Amzallag, I. Baraille, M. Rérat, *Phys. Rev. B* **2006**, *74*, 195123/1-8.
[55] A. Paleari, V. N. Sigaev, N. V. Golubev, E. S. Ignat'eva, S. Bracco, A. Comotti, A. Azarbod and R. Lorenzi, *Acta Mater.*, 2014, **70**, 19-29.
[56] J. A. Duffy, *J. Sol. St. Chem.*, 1986, **62**, 145-157.
[57] V. Dimitrov and T. Komatsu, *J. Univ. Chem. Tech. Metallurgy*, 2010, **45**, 219-250.
[58] M. Chavoutier, D. Caurant, O. Majérus, R. Boulesteix, P. Loiseau, C. Jousseaume, E. Brunet and E. Lecomte, *J. Non-Cryst. Sol.*, 2014, **384**, 15-24.
[59] E. Fois, A. Gamba and G. Tabacchi, *Chem. Phys. Chem.*, 2008, **9**, 538-543.
[60] J. R. Lakowicz, *Principles of Fluorescence Spectroscopy (3rd edition)*, Springer, 2006, Chapter 2.9.4.

Entry for the Table of Contents

ARTICLE

Donor-acceptor nano-balance: In wide-band-gap Ga-oxide nanocrystals in glass, the main players of the light-emitting material – i.e. donor-acceptor species – find their final place and functional role thanks to driving forces which are influenced by Ga-substituting Ni or Ti ions. As a result, a chain of effects can control donor-acceptor balance and give a strategy to design light-emission of grown-in-glass nano-phases (see picture).

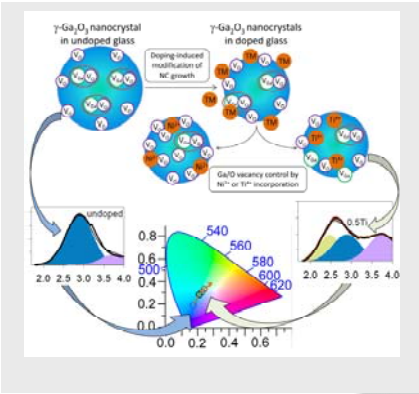

Alberto Paleari, Nikita V. Golubev, Elena S. Ignat'eva, Vladimir N. Sigaev, Roberto Lorenzi,*

Page No. – Page No.

Donor-acceptor control in grown-in-glass Ga-oxide nanocrystals by crystallization-driven heterovalent doping

S1. Analysis of the role of Ni and Ti doping in the Kroger-Vink notation

The effects of Ni^{2+} and Ti^{4+} ions substituting for Ga^{3+} in octahedral sites in NCs (pictorially displayed in Figure 1) are described in more detail using the Kroger-Vink notation. For sake of simplicity, herein and in the paper, we neglect to write the superscript *X* to indicate the neutral state of elements and single vacancies. With the only aim of representing some of the possible mechanisms of doping-induced perturbation of the local charge compensation at Ga_2O_3 defect sites and complexes, Equations (1)-(3) (and (4)-(6)) analyze three NiO (and TiO_2) concentrations corresponding to the doping levels in the investigated materials. The final step of each equation is a simplified scheme of the evolution of the system after trapping of photo-excited electrons from the conduction band and subsequent radiative decay. The first three equations regards NiO doping:

0.05 mol% NiO
$$2\left[\begin{matrix}V_O^{\cdot}\\(V_O^{\cdot\cdot},V_{Ga}^{\prime\prime\prime})^{\prime}\end{matrix}\right]^X + Ni \rightarrow \left[\begin{matrix}V_O^{\cdot}\\(V_O^{\cdot\cdot},V_{Ga}^{\prime\prime\prime})^{\prime}\end{matrix}\right]^X + \left[\begin{matrix}V_O^{\cdot}\\V_O,Ni_{Ga}^{\prime}\end{matrix}\right]^X$$
$$\xrightarrow{\substack{photoexcitation\\and\ optical\ decay}} \left(\left[\begin{matrix}V_O^{\cdot}\\(V_O^{\cdot\cdot},V_{Ga}^{\prime\prime\prime})^{\prime}\end{matrix}\right]^X + h\nu_{blue}\right) + \left(\left[\begin{matrix}V_O^{\cdot}\\V_O,Ni_{Ga}^{\prime}\end{matrix}\right]^X + h\nu_{UV}\right) \quad (1)$$

0.10 mol% NiO
$$2\left[\begin{matrix}V_O^{\cdot}\\(V_O^{\cdot\cdot},V_{Ga}^{\prime\prime\prime})^{\prime}\end{matrix}\right]^X + 2Ni + V_{Ga} \rightarrow \left[\begin{matrix}V_O^{\cdot}\\(V_O^{\cdot\cdot},V_{Ga}^{\prime\prime\prime})^{\prime}\end{matrix}\right]^X + \left[\begin{matrix}V_O^{\cdot},Ni_{Ga}\\V_O,Ni_{Ga}^{\prime}\end{matrix}\right]^X$$
$$\xrightarrow{\substack{photoexcitation\\and\ optical\ decay}} \left(\left[\begin{matrix}V_O^{\cdot}\\(V_O^{\cdot\cdot},V_{Ga}^{\prime\prime\prime})^{\prime}\end{matrix}\right]^X + h\nu_{blue}\right) + (2[V_O^{\cdot},Ni_{Ga}^{\prime}]^X + h\nu_{UV}) \quad (2)$$

0.50 mol% NiO
$$2\left[\begin{matrix}V_O^{\cdot}\\(V_O^{\cdot\cdot},V_{Ga}^{\prime\prime\prime})^{\prime}\end{matrix}\right]^X + 10Ni + 9V_{Ga} + 8V_O \rightarrow \left[\begin{matrix}V_O^{\cdot}\\(V_O^{\cdot\cdot},V_{Ga}^{\prime\prime\prime})^{\prime}\end{matrix}\right]^X + \left[\begin{matrix}V_O^{\cdot},Ni_{Ga}\\V_O,Ni_{Ga}^{\prime}\end{matrix}\right]^X + 8[V_O,Ni_{Ga}]^X$$
$$\xrightarrow{\substack{photoexcitation\\and\ optical\ decay}} \left(\left[\begin{matrix}V_O^{\cdot}\\(V_O^{\cdot\cdot},V_{Ga}^{\prime\prime\prime})^{\prime}\end{matrix}\right]^X + h\nu_{blue}\right) + (10[V_O^{\cdot},Ni_{Ga}^{\prime}]^X + h\nu_{UV}) \quad (3)$$

In equations (1) and (2), the oxygen defectiveness is supposed fixed, whereas equation (3) accounts for additional V_O sites which are induced by the large number of Ni sites which overcomes the quantity of native V_O in undoped material. The number of V_{Ga} sites is adjusted so as to formally express Ga substitution by Ni doping.

Analogously, but with some relevant differences, equations (4)-(6) analyze some of the possible local effects of Ti^{4+} incorporation substituting for Ga^{3+} ions in NCs. In particular, based on PL data, equations (4) to (6) account for a higher propensity of Ti^{4+} with respect to Ni^{2+} to prevent the formation of $[V_O,V_{Ga}]$ complexes which act as acceptor sites in blue luminescence (a possible mechanism, for instance, may be a preferential Ti^{4+} placement not far from V_{Ga} sites, so as to hinder complexes with oxygen vacancies):

0.05 mol% TiO_2
$$2\left[\begin{matrix}V_O^{\cdot}\\(V_O^{\cdot\cdot},V_{Ga}^{\prime\prime\prime})^{\prime}\end{matrix}\right]^X + Ti \rightarrow \left[\begin{matrix}V_O^{\cdot}\\(V_O^{\cdot\cdot},V_{Ga}^{\prime\prime\prime})^{\prime}\end{matrix}\right]^X + \left[\begin{matrix}2V_O\\Ti_{Ga}\end{matrix}\right]^X$$
$$\xrightarrow{\substack{photoexcitation\\and\ optical\ decay}} \left(\left[\begin{matrix}V_O^{\cdot}\\(V_O^{\cdot\cdot},V_{Ga}^{\prime\prime\prime})^{\prime}\end{matrix}\right]^X + h\nu_{blue}\right) + \left(\left[\begin{matrix}2V_O\\Ti_{Ga}\end{matrix}\right]^X + h\nu_{UV}\right) \quad (4)$$

0.10 mol% TiO_2 $$2\left[\begin{matrix}V_O^{\cdot}\\(V_O^{\cdot\cdot},V_{Ga}^{'''})'\end{matrix}\right]^X + 2Ti + 2V_{Ga} \rightarrow \left[\begin{matrix}V_O^{\cdot}\\(V_O^{\cdot\cdot},V_{Ga}^{'''})'\end{matrix}\right]^X + \left[\begin{matrix}2V_O\\V_{Ga},2Ti_{Ga}\end{matrix}\right]^X$$

$$\xrightarrow{\substack{photoexcitation\\and\ optical\ decay}} \left(\left[\begin{matrix}V_O^{\cdot}\\(V_O^{\cdot\cdot},V_{Ga}^{'''})'\end{matrix}\right]^X + h\nu_{blue}\right) + \left(\left[\begin{matrix}2V_O\\V_{Ga},2Ti_{Ga}\end{matrix}\right]^X + h\nu_{UV} + h\nu_{green}\right) \quad (5)$$

0.50 mol% TiO_2 $$2\left[\begin{matrix}V_O^{\cdot}\\(V_O^{\cdot\cdot},V_{Ga}^{'''})'\end{matrix}\right]^X + 10Ti + 10V_{Ga} \rightarrow \left[\begin{matrix}V_O^{\cdot}\\(V_O^{\cdot\cdot},V_{Ga}^{'''})'\end{matrix}\right]^X + \left[\begin{matrix}2V_O\\V_{Ga},10Ti_{Ga}\end{matrix}\right]^X$$

$$\xrightarrow{\substack{photoexcitation\\and\ optical\ decay}} \left(\left[\begin{matrix}V_O^{\cdot}\\(V_O^{\cdot\cdot},V_{Ga}^{'''})'\end{matrix}\right]^X + h\nu_{blue}\right) + \left(\left[\begin{matrix}2V_O\\V_{Ga},10Ti_{Ga}\end{matrix}\right]^X + h\nu_{UV} + h\nu_{green}\right) \quad (6)$$

Equations (5) and (6) also account for additional V_{Ga} sites which are induced by the large number of Ti sites.

S2. X-ray diffraction data of doped and undoped samples after heating up to 960 °C

The thermal evolution of γ-Ga_2O_3 nanocrystals in alkali-germanosilicate glasses proceeds from the crystallization temperature T_{exo} through the diffusion of lithium from the glass to the nanocrystals with the formation of a nanophase close to $LiGa_5O_8$, which then undergoes decomposition at T_{endo} – activated by a high temperature order-disorder transformation of the $LiGa_5O_8$ phase [Datta, R. K. *J. Am. Ceram. Soc.* **1971**, 54, 262.] – finally forming β-Ga_2O_3 NCs [Ref. 46]. The size of the $LiGa_5O_8$ NCs before final transformation at T_{endo} is larger than the initial size of γ-Ga_2O_3 NCs grown in the glass matrix, and it provides a higher sensitivity to disorder effects thanks to much narrower and more defined reflections in the XRD pattern.

In Figures S1 and S2 we report the XRD patterns of glassceramics with molar composition $7.5Li_2O$–$2.5Na_2O$–$20Ga_2O_3$–$25GeO_2$–$45SiO_2$ doped with different NiO or TiO_2 content, as exposed in the paper, after treatment with the same heating rate as in DSC measurements from room temperature up to 960 °C. The patterns are compared with the patterns of $LiGa_5O_8$ (PDF 01-076-0199) and of defective $Li_{0.51}[Li_{0.462}Ga_{0.54}][Ga_{4.484}O_8]$ (PDF 01-086-0649).

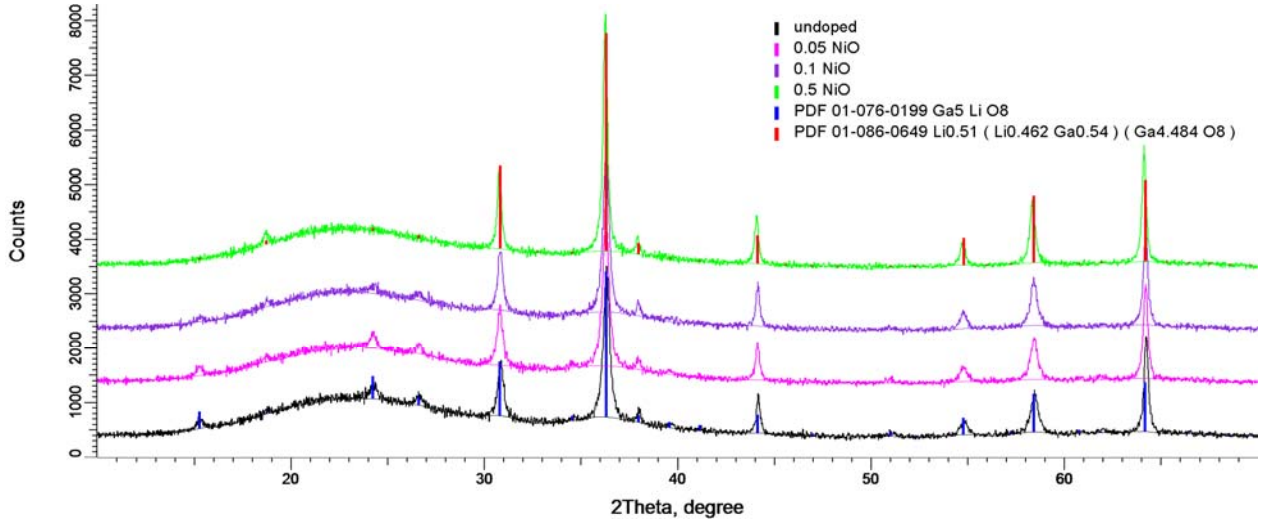

Fig. S1. XRD patterns of glass with molar composition $7.5Li_2O$–$2.5Na_2O$–$20Ga_2O_3$–$25GeO_2$–$45SiO_2$ with different NiO. The patterns are shifted for clarity. Samples were treated with the same heating rate as in DSC measurements from room temperature up to 960 °C.

The decrease of Bragg's reflection intensities at about 15.3, 24.2, and 26.6° at increasing NiO content indicates that $LiGa_5O_8$ with deviation from stoichiometry fits better the XRD pattern of NiO doped glass than stoichiometric $LiGa_5O_8$. This fact supports the idea that heavy doping induces a larger defectiveness. This effect is less pronounced for TiO_2-doped glasses (see XRD patterns below) probably because a fraction of TiO_2 stays in the glass.

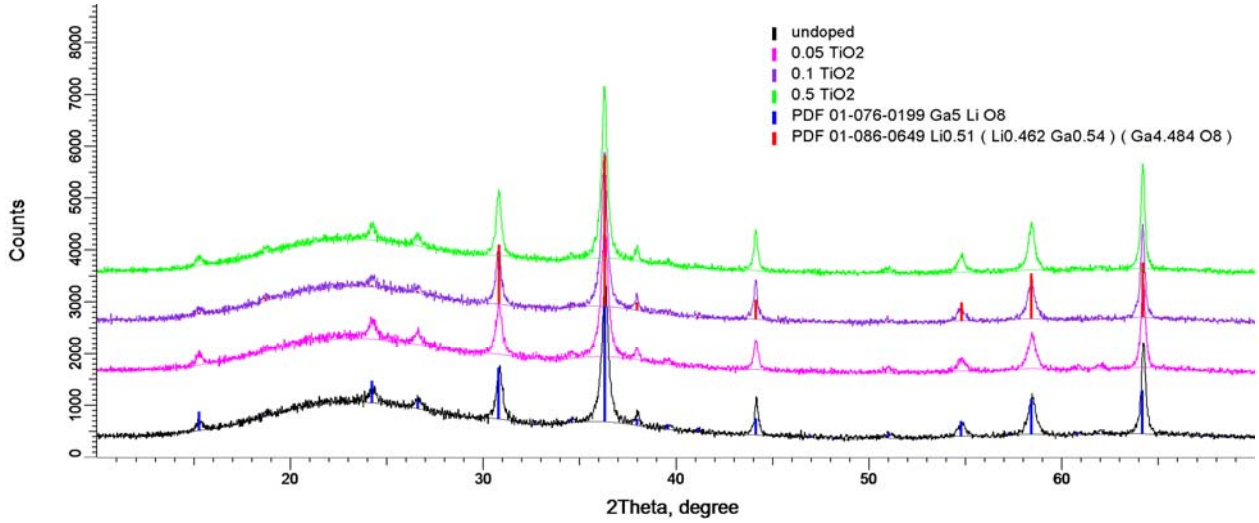

Fig. S2. XRD patterns of glass with molar composition $7.5Li_2O–2.5Na_2O–20Ga_2O_3–25GeO_2–45SiO_2$ with different TiO_2. The patterns are shifted for clarity. Samples were treated with the same heating rate as in DSC measurements from room temperature up to 960 °C.

S3. Experiment supporting the role of changes of V_O content on the light emission modifications

The results we describe in the paper show that NiO and TiO_2 addition in nanostructured glass with composition $7.5Li_2O$-$2.5Na_2O$-$20Ga_2O_3$-$45GeO_2$-$25SiO_2$ (mol%) modifies spectral distribution and integrated intensity of nanocrystal (NCs) light emission. We also show that the analysis of various kinds of data indicates that the modified properties are ascribable to the effect of Ni^{2+} and Ti^{4+} incorporation in NCs on oxygen and Ga vacancies. These sites are in fact responsible, according to previous studies, for different photoluminescence (PL) components in the UV, blue, and green regions, depending on their relative population and formation of related complexes acting either as light emitting single centres or pairs of donor and acceptor sites. We report below the results of an additional experiment which provides an additional and independent indication that the responsible optical active centres are strictly related to the oxygen stoichiometry. Specifically, the experiment shows that applying reducing conditions during the melting procedure of undoped material – without addition of NiO or TiO_2 – causes modifications of the PL spectrum of the final nanostructured material analogous to the spectral changes observed by doping.

A set of samples were prepared with composition $7.5Li_2O$-$2.5Na_2O$-$20Ga_2O_3$-$45GeO_2$-$25SiO_2$ (mol%), without NiO or TiO_2 addition, with the same method described in the paper, except for the conditions during the melting procedure. A fraction of the material was obtained in unperturbed melting conditions, similarly to doped materials. Another fraction was obtained modifying the melting conditions with activated carbon, adding a tablet of 250 mg onto the melt at intervals of 10 min, for a total of 1 g of active

carbon. The resulting glasses were then treated at the crystallization temperature for each batch. We report in Fig. S3 PL spectra of the obtained samples. The dependence of the distribution of PL intensity on the reducing conditions during melting confirms the interpretation of the effects of NiO or TiO_2 doping as the result of Ni^{2+} and Ti^{4+} on the NC oxygen stoichiometry. Oxygen deficient samples show more intense contribution in the UV region and depleted blue component. In this case, the occurrence of a green independent component is well detectable, especially exciting at 350 nm.

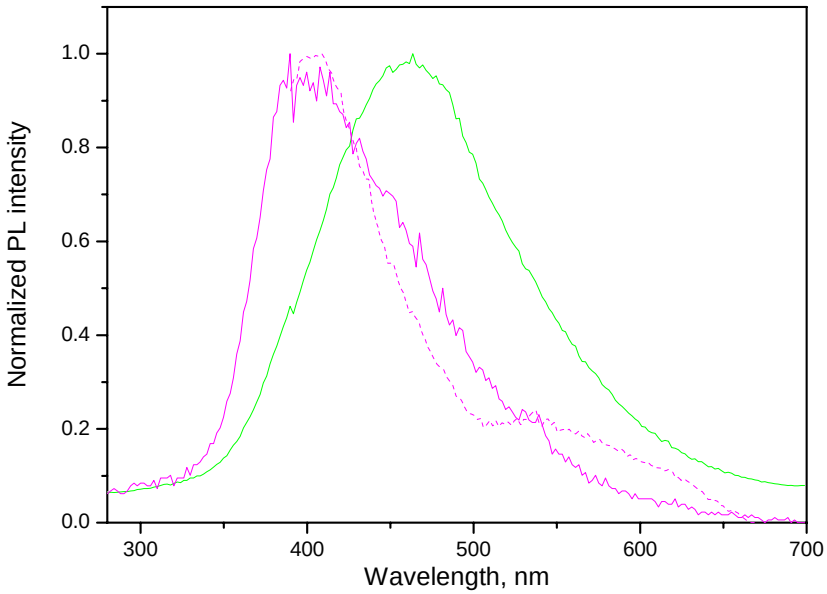

Fig. S3. PL spectra of nanostructured undoped glassceramics obtained by heating at crystallization temperature $7.5Li_2O$-$2.5Na_2O$-$20Ga_2O_3$-$45GeO_2$-$25SiO_2$ (mol%) glasses prepared in unperturbed melting conditions (green curve, excited at 250 nm) and with addition of carbon as reducing agent (violet curve, excited at 250 nm; dashed violet curve, excited at 350 nm).